



UNIVERSITY OF LEEDS

This is a repository copy of *Enhanced Spin–Orbit Coupling in Heavy Metals via Molecular Coupling*.

White Rose Research Online URL for this paper:
<https://eprints.whiterose.ac.uk/170836/>

Version: Accepted Version

Article:

Alotibi, S, Hickey, BJ, Teobaldi, G et al. (11 more authors) (2021) Enhanced Spin–Orbit Coupling in Heavy Metals via Molecular Coupling. *ACS Applied Materials & Interfaces*, 13 (4). pp. 5228-5234. ISSN 1944-8244

<https://doi.org/10.1021/acsami.0c19403>

© 2021 American Chemical Society. This is an author produced version of a journal article published in *ACS Applied Materials & Interfaces*. Uploaded in accordance with the publisher's self-archiving policy.

Reuse

Items deposited in White Rose Research Online are protected by copyright, with all rights reserved unless indicated otherwise. They may be downloaded and/or printed for private study, or other acts as permitted by national copyright laws. The publisher or other rights holders may allow further reproduction and re-use of the full text version. This is indicated by the licence information on the White Rose Research Online record for the item.

Takedown

If you consider content in White Rose Research Online to be in breach of UK law, please notify us by emailing eprints@whiterose.ac.uk including the URL of the record and the reason for the withdrawal request.



eprints@whiterose.ac.uk
<https://eprints.whiterose.ac.uk/>

Enhanced spin-orbit coupling in heavy metals via molecular coupling

Satam Alotibi¹, Bryan J. Hickey¹, Gilberto Teobaldi^{2,3,4,5}, Mannan Ali¹, Joseph Barker¹, Emiliano Poli², David D. O'Regan^{6,7}, Quentin Ramasse^{1,8}, Gavin Burnell¹, James Patchett⁹, Chiara Ciccarelli⁹, Mohammed Alyami¹, Timothy Moorsom¹ and Oscar Cespedes^{1}*

¹*School of Physics and Astronomy, University of Leeds, Leeds LS2 9JT, U.K..*

²*Scientific Computing Department, Science and Technology Facilities Council, Didcot OX11 0QX, U.K.*

³*Beijing Computational Science Research Center, 100193 Beijing, China*

⁴*Stephenson Institute for Renewable Energy, Department of Chemistry, University of Liverpool, L69 3BX Liverpool, U.K.*

⁵*School of Chemistry, University of Southampton, Highfield, SO17 1BJ Southampton, U.K.*

⁶*School of Physics, Trinity College Dublin, The University of Dublin, Dublin 2, Ireland*

⁷*Centre for Research on Adaptive Nanostructures and Nanodevices (CRANN) and the SFI Advanced Materials and Bio-Engineering Research Centre (AMBER), Dublin 2, Ireland*

⁸*SuperSTEM, SciTech Daresbury Science and Innovation Campus, Keckwick Lane, Daresbury WA4 4AD, U.K.*

⁹*Cavendish Laboratory, University of Cambridge, JJ Thomson Avenue, Cambridge CB3 0HE, U.K.*

KEYWORDS: Metallo-Molecular Interfaces, Spin Orbit Interaction, Yttrium Iron Garnet, Emergent Functionalities, Spin Hall angle, Molecular Spintronics, Charge Transfer.

ABSTRACT

5d metals are used in electronics because of their high spin-orbit coupling (SOC) leading to efficient spin-electric conversion. When C_{60} is grown on a metal, the electronic structure is altered due to hybridisation and charge transfer. In this work we measure the spin Hall magnetoresistance for Pt/ C_{60} and Ta/ C_{60} , finding they are up to a factor 6 higher than for the pristine metals, indicating an increase in spin Hall angle of 20-60%. At low fields of 1-30 mT the presence of the C_{60} increased the anisotropic magnetoresistance by up to 700%. Our measurements are supported by non-collinear Density Functional Theory calculations, which predict a significant SOC enhancement by C_{60} that penetrates through the Pt layer, concomitant with trends in the magnetic moment of transport electrons acquired via SOC and symmetry breaking. The charge transfer and hybridisation between the metal and the C_{60} can be controlled by gating, so our results indicate the possibility of dynamically modifying the SOC of thin metals using molecular layers. This could be exploited in spin transfer torque memories and pure spin current circuits.

INTRODUCTION

The spin-orbit interaction is perhaps the most crucial mechanism to be optimised in the design of magnetic structures and metal device physics. It determines the magnetocrystalline anisotropy, is key to the propagation and electrical conversion of spin currents, determines the magnitude of interfacial mechanisms such as the Dzyaloshinskii–Moriya interaction and has opened new paths of research, such as the generation of Majorana fermions and energy band engineering of topological insulators¹⁻⁵. The SOC also controls the efficiency of spin - charge conversion in the spin Hall, spin torque and spin Seebeck effects. All of these are important for reducing the power consumption and energy dissipation of computing and electronic devices—an issue at the forefront of technology development. However, the SOC can currently only be tuned by static means, such as doping, preventing the design of architectures where spin, charge and magnetic interactions can be reversibly modified to enhance device performance or to acquire new functionalities. There are however preliminary reports that point to the possibility of gating the interfacial Rashba SOC⁶.

The Spin Hall magnetoresistance (SHMR) can be used to quantify the SOC in systems such as thin (~nm) heavy metal layers deposited on a magnetic insulator, such as the yttrium iron garnet $\text{Y}_3\text{Fe}_5\text{O}_{12}$ (YIG)⁷⁻⁹. When an electric current, \mathbf{J}_c , flows in the metal, the spin Hall effect (SHE) induces a perpendicular spin current, \mathbf{J}_s , with the spin polarization, s , parallel to the film surface. If the YIG magnetization, \mathbf{M} , is parallel to s , \mathbf{J}_s cannot flow into the magnet and a spin accumulation forms. The resistance is the same as a bare Pt wire. When \mathbf{M} is not parallel to s , the transverse component exerts a torque on the YIG magnetic moments, injecting spin current into the magnet. This opens a dissipation channel for the spin current, reducing the inverse SHE contribution to \mathbf{J}_c and the resistance of Pt appears to increase^{5, 10}. The dissipation is largest when \mathbf{M} is perpendicular to s and the maximum SHMR should occur. The SHMR is measured by rotating

the angle β in Fig. 1a, with the applied \mathbf{H} field (and therefore \mathbf{M}) always orthogonal to the electrical current, but varying from in-plane to out-of-plane, and therefore from parallel (R_{\min}) to perpendicular to the spin polarization (R_{\max})^{5, 11-12}.

The ratio of the spin to charge current is known as the spin Hall angle: $\theta_{SH} = |\mathbf{J}_s|/|\mathbf{J}_c|$ ¹³⁻¹⁵. θ_{SH} is important in devices such as spin transfer torque (STT) memories as it is correlated with the torque exerted on ferromagnets¹⁶. A larger SHMR indicates an increased θ_{SH} which makes spin transfer torques larger, reducing the switching currents (and therefore power consumption) of STT memory devices. By using a molecular layer to tune the effective SOC in conventional magnetic insulator/metal structures, we can differentiate spin transport effects based on their physical origins¹⁷⁻¹⁸.

At metallo-molecular interfaces, the electronic and magnetic properties of both materials change due to charge transfer and hybridisation¹⁹⁻²². This can cause spin ordering and spin filtering²³⁻²⁶, or change the magnetic anisotropy^{22, 27-28}. Even though composed of light carbon, fullerenes with large curvature can produce a large spin-electrical conversion^{2, 29-31}. Here, we study the effect of metal/ C_{60} interfaces on the SHMR and anisotropic magnetoresistance (AMR) of YIG/Pt and YIG/Ta. We aim to: investigate the mechanisms behind spin orbit scattering at hybrid metal/ C_{60} interfaces, maximise technologically-relevant parameters, and provide a pathway towards the dynamic electrical tuning of SOC.

EXPERIMENTAL

Using shadow mask deposition, we grew two metal wires simultaneously on the same YIG substrate and, without breaking vacuum, covered one wire with 50 nm of C₆₀ –modifying the density of states (DOS) and transport properties of the metal. According to our density functional theory (DFT) calculations for Pt/C₆₀, 0.18-0.24 electrons per C₆₀ molecule are transferred, and the first molecular layer is metallised. This reduces the electron surface scattering, improving the residual resistance ratio (RRR) –Fig. 1b and Supplementary Information. Our Ta wires have a resistivity (~1-2 μΩ·m) and a negative temperature coefficient (~-500·10⁻⁶ K⁻¹), consistent with a sputtered β-Ta phase³². For Ta, C₆₀ increases the resistivity, the opposite of the effect on Pt–see Fig. 1b.

The change in resistivity as the magnetic field is rotated is fitted to a cos²(β) function—the amplitude is the SHMR. When the magnetisation is saturated by the applied field the SHMR also saturates. This occurs for an out-of-plane field of 0.1-0.15 T for a YIG film 170 nm thick at 290 K, and no higher than 0.5 T for any measured condition. For fields greater than 0.5 T, other contributions such as Koehler MR, localisation and the Hanle effect can result in significant linear and parabolic contributions to the MR that would artificially enhance the SHMR ratio and θ_{SH} (Fig. 1c)³³. For a YIG/Pt(2nm) sample, the C₆₀ layer increases the MR by roughly a factor of 3, due to spin accumulation, but the polynomial contributions reduce because of the increased effective (conducting) thickness of the Pt/C₆₀ bilayer. In YIG/Ta(4nm), where C₆₀ increases the resistance rather than reducing it, both the SHMR up to 0.15 T and the polynomial MR at higher fields are enhanced (Fig. 1d).

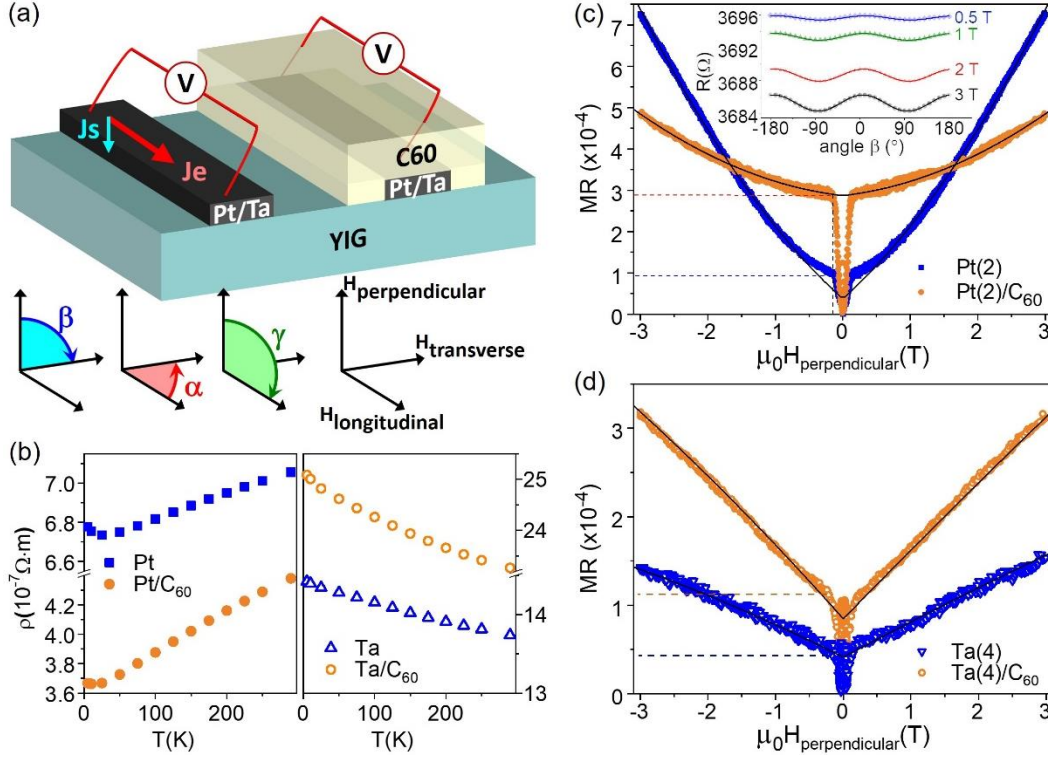


Figure 1 (a) Schematic of the experiment. There are three possible orientations of the magnetic field (H) w.r.t. the electrical current and the YIG film. To measure the SHMR without contributions from the AMR effect, we rotate H from perpendicular to transverse (change in β). (b) Typical resistivity of thin Pt (3 nm) and Ta (4 nm) wires on YIG. With C_{60} on top, the Pt resistivity is about 40% lower, the RRR factor increases and the upturn at low T is absent. With Ta, we observe the opposite effect, an increase in the resistivity with the molecular interface. (c) MR in a Pt wire with $H_{\text{perpendicular}}$. The spin Hall contribution to the MR at 300 K reaches a maximum at ~ 0.1 - 0.15 T, where the YIG film is saturated out of plane. Inset: Resistance with different applied fields as a function of the angle β . The data is fitted to a $\cos^2(\beta)$ function. We take the amplitude at the lowest field of 0.5 T, when the YIG substrate is saturated but the polynomial contributions are small, as the SHMR value. (d) MR in a Ta wire with $H_{\text{perpendicular}}$ at 75 K. The maximum in the spin Hall contribution at this temperature is reached at ~ 0.2 T.

RESULTS

The SHMR values at 0.5 T for Pt and Pt/C₆₀ are plotted in Fig. 2a, and the ratios with and without a molecular overlayer in Fig. 2b. The temperature dependence of the SHMR reproduces observations in RF-sputtered YIG/sputtered Pt wires³³. For Pt grown by evaporation on thicker, liquid epitaxy or pulsed laser deposition YIG, the SHMR has a gentler drop at high temperatures. This is attributed to a smaller temperature dependence of the spin diffusion length³⁴⁻³⁵, which could be due to a different resistivity of Pt and different magnetic behaviour of YIG films depending on the growth method. It is possible that the larger SHMR observed in metallo-molecular wires could be due to a change in the spin mixing conductance ($G^{\uparrow\downarrow}$) induced by C₆₀^{7,36}. However, $G^{\uparrow\downarrow}$ is related to the spin transparency of the YIG/Pt interface, where the effect of the molecular interface is small. Also, we do not observe an increase in the ferromagnetic resonant damping α (which is proportional to $G^{\uparrow\downarrow}$) for YIG/Pt when the C₆₀ layer is present (Fig. 2c)³⁷. Furthermore, our results for the change in SHMR with temperature cannot be fitted by changing $G^{\uparrow\downarrow}$ without also changing θ_{SH} . We assume the spin mixing conductance is $G^{\uparrow\downarrow}=4\times 10^{14} \Omega^{-1}\text{m}^{-2}$ ⁹, Fig. 2c shows θ_{SH} deduced from fitting the SHMR (see Supporting Information for other fitting values^{34,38}). For Pt wires of ≤ 5 nm, there is an increase in θ_{SH} with C₆₀. The effect disappears for thick wires (> 10 nm), where the molecular interface does not significantly change the spin Hall angle. A similar molecular enhancement of the SHMR and θ_{SH} is observed for Ta wires.

Molecules may affect the Rashba effect and spin texture of the metal, leading to changes in the effective SOC of the hybrid wire³⁹⁻⁴¹. Our DFT simulations rule out mechanisms based on the formation of a perpendicular dipole which arises due to charge transfer at the Pt/C₆₀ interface and its associated potential step, which breaks the symmetry⁴². This induced dipole is maximised at 2.5 nm, where the experiments show a local minimum in the enhancement of θ_{SH} .

Our DFT simulations do not explicitly calculate SHMR or transversal spin-separation or accumulation, but they do reveal that net magnetic moments can be acquired by Pt electrons. This will make the charge flow spin-dependent, given time-reversal symmetry breaking. The magnitude of the induced magnetic moments follows the experimental trends with Pt film thickness (Fig. S15). Additional analysis of thermally or disorder-activated inter-band transitions *and* normal intra-band coherent spin transport based on the non-collinear DFT band-structures (Fig. S16) confirms an inverse relationship between the C_{60} enhanced magnetic moments and the thickness of the Pt slab. The main result from DFT is the strength of the SOC term in the Hamiltonian—the sum of the orbital matrix elements which is denoted E_{SOC} . Figs. 2d and e show the net and fractional change of this energy for each layer of Pt when C_{60} is included in calculations. The first two Pt layers directly beneath the C_{60} experience a marked decrease in SOC strength. Further from the C_{60} interface there is a rebound and net enhancement in the third, fourth and fifth Pt layers. These layers are further away from the C_{60} and closer to the interface with YIG. As per Fig. S11, the percentage increase per Pt layer induced by the C_{60} (compared to the same layer in the bare Pt(111) slab) is substantial and as large as 10-20% for the thinnest (1.1 nm) slab. Intriguingly, this multiplicative enhancement persists deep within the Pt, albeit reduced by factor of roughly 2 in the bottommost (YIG-facing) layers of the thicker (2.5 nm and 3.9 nm) slabs. As a result of these trends, the Pt layers with the largest SOC enhancement (the 1.1 nm sample) are in direct proximity to the YIG. In contrast, in thicker 2.5 nm and 3.9 nm slabs, the Pt-layers with the largest SOC (#3, 4, 5) are located progressively farther from the YIG interface, resulting in progressively smaller enhancement of θ_{SH} . But the enhancement is present for all slab thickness modeled (up to 3.9 nm in Fig. 2c). Thus, we hypothesise that it is the long-ranged, yet thickness dependent, C_{60} -induced SOC enhancement that ultimately enables non-trivial spin-conduction in the system.

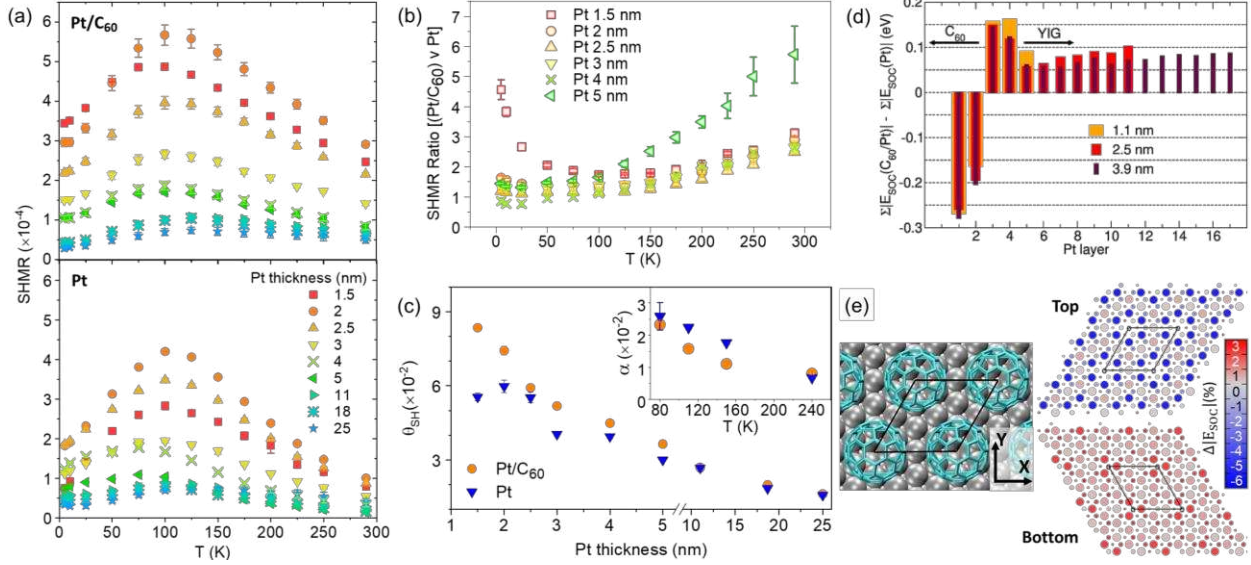


Figure 2. (a) SHMR for Pt and equivalent Pt/C₆₀ wires of different thicknesses on GGG/YIG(170 nm) films. (b) SHMR ratios between Pt/C₆₀ and Pt. The maximum effect of the molecular layer (a factor of 4 to 7 change) takes place for thin films (1.5 nm) at low temperatures or thick films (5 nm) at room temperature. (c) For wires ≤ 5 nm, θ_{SH} obtained from the SHMR data fitting is significantly higher with the molecular overlayer. Inset: the magnetic resonance damping α is not increased by the C₆₀ interface; here a comparison of YIG/Pt/Al/C₆₀ and YIG/Pt/C₆₀ shows similar or even higher damping values for the decoupled YIG/Pt/Al/C₆₀ sample. (d) Pt-layer resolved, calculated C₆₀-induced changes in SOC strength (ΔE_{SOC}) as a function of the thickness of the Pt-slab. Pt layer 1 is the closest to the C₆₀. (e) Top view of the optimized C₆₀/Pt(111)-(2 $\sqrt{3}$ x2 $\sqrt{3}$)R30° interface DFT model. The C₆₀ molecules are adsorbed on top of one Pt-vacancy. The black polygon marks the in-plane periodicity of the system. Pt: silver, C: cyan. Right: Pt-atom resolved 2D-maps of the C₆₀-induced changes in E_{SOC} ($\Delta|E_{SOC}|$) for the three topmost (top) and bottommost (bottom) Pt-layers in C₆₀/Pt (1.1 nm).

The fabrication of YIG films can lead to elemental diffusion and defects that change the magnetic properties of the ferrimagnet and the interpretation of transport measurements⁴³. Figs. 3a-b show atomic-resolution aberration corrected cross-sectional scanning transmission electron microscopy (STEM) images and electron energy loss spectroscopy (EELS) chemical maps. It is possible to observe, in addition to a certain level of surface roughness of the YIG film, an area close to the YIG surface and below the sputtered Pt wire into which some Pt metal may have diffused and formed a low density of nm-sized clusters (see also Fig. S4 in Supp. Inf.). This diffusion can affect the magnetization and anisotropy direction at the surface of the YIG layer, giving rise to the minor loops we observe in the perpendicular field direction in some YIG films⁴³.

For Pt grown on YIG, an additional change in resistance is observed at low magnetic fields <5-20 mT when the direction of an applied magnetic field is changed with respect to the electrical current. The origin of this AMR is controversial. It has been attributed to a proximity-induced magnetization of Pt, which is close to the Stoner criterion, but it is also claimed that there is no evidence for this induced magnetization¹⁷⁻¹⁸. The same effect is also seen in YIG/Ta. This low field AMR (LF-AMR) is characterized by the presence of peaks, positive or negative depending on the field direction, resembling the AMR observed in magnetic films with domain wall scattering⁴⁴⁻⁴⁵. Due to the SOC, in most magnetic materials domain walls reduce the resistance for in-plane fields, and increase it for out of plane fields. This domain wall AMR peaks at the coercive field H_c of the magnet, for the greatest magnetic disorder and domain wall density. In YIG/Pt, the position of out-of-plane LF-AMR peaks coincides with the coercivity of the perpendicular minor YIG loops (Fig. 3c and Supp. Inf.), which could point to a YIG surface layer with an out-of-plane easy axis.

We find that the LF-AMR has the same shape and peak position with or without a molecular overlayer. However, the magnitude of the LF-AMR is larger when C₆₀ is present. This molecular effect is stronger for the perpendicular configuration (Fig. 3d), which may be due a larger perpendicular magnetic anisotropy induced by C₆₀, as reported for Co²². A larger LF-AMR is also observed in YIG/Ta when C₆₀ is deposited on top [40]. For YIG films grown on YAG substrates, the in-plane coercivity is increased by 1-2 orders of magnitude, and the LF-AMR peaks appear at higher fields, supporting the correlation between the AMR in Pt and the surface YIG magnetisation (Figs. S5-S7 in Supplementary Information).

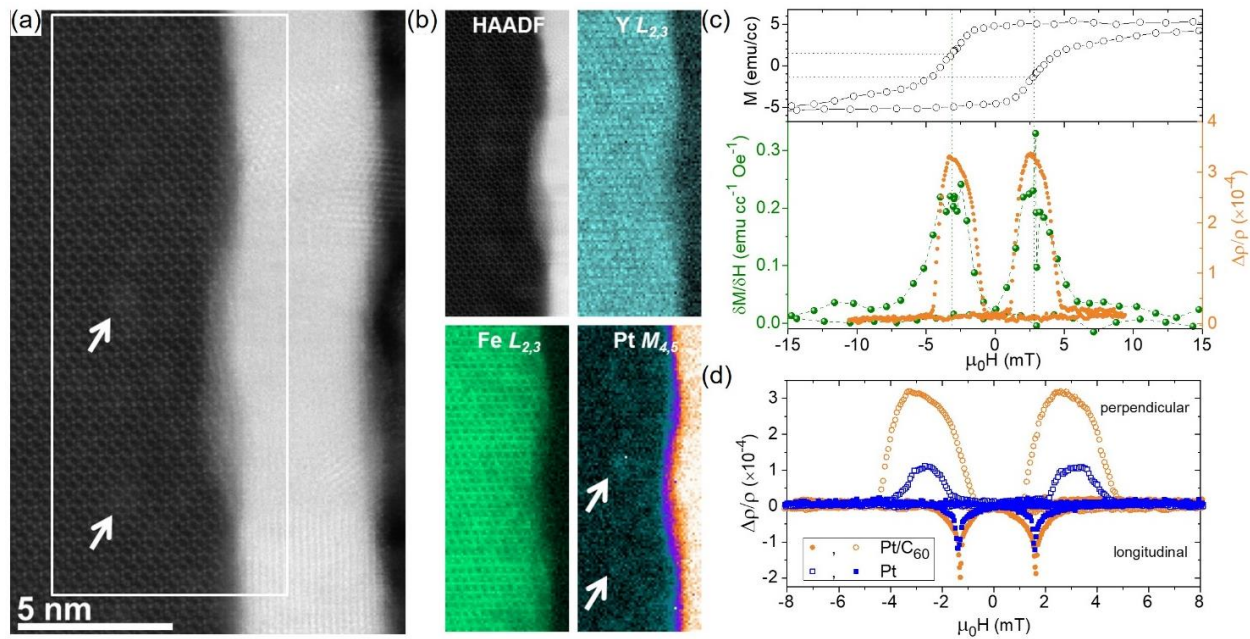


Figure 3. (a) Cross-sectional high angle annular dark field (HAADF) image of the YIG/Pt interface using scanning transmission electron microscopy (see methods in Supp. Inf. for details). (b) Elemental chemical analysis of the interface using EELS: the relative intensity maps of the Y, Fe and Pt ionization edges are presented with a simultaneously acquired HAADF image of the region, indicated by a white box in (a). Bright clusters immediately below the YIG surface, indicated by white arrows in the Pt map and the overview HAADF image, contain a higher Pt concentration and may be due to Pt diffusion into the YIG. (c) Low field MR and minor hysteresis loop with the field in the perpendicular orientation at 200 K. The full loop uncorrected and other examples can be found in the Supplementary Information. (d) Room temperature LF-AMR comparison between YIG/Pt and YIG/Pt/C₆₀. The curves are qualitatively the same, but the magnitude of the effect is enhanced by the molecules.

The LF-AMR peak position (coercivity of the YIG surface) and peak width (saturation field of the YIG surface), increase as the temperature is lowered (Figs. 4a-b). Typically, the AMR of YIG/Pt measured at high fields is reported to vanish above 100-150 K. If measuring at 3 T, where quantum localisation and other effects are strong, we observe this same decay with temperature. However, the LF-AMR can be observed up to room temperature. C_{60} not only increases the LF-AMR value, but it also makes it less temperature dependent, so that the LF-AMR ratio can be up to 700% higher for Pt/ C_{60} at 290 K. This supports our suggestion from DFT simulations of a mechanism based on C_{60} -induced re-hybridization enhancing the magnetic moment acquired by transport electrons via SOC (Fig. 4c).

The LF-AMR depends on the Pt thickness, t , as $(t - x)^{-1}$ (Fig. 4d). We identify the value of x , approximately 1 nm, as the magnetised Pt region contributing to the AMR. This relationship is not affected by the C_{60} layer, although the magnitude is uniformly higher with molecules.

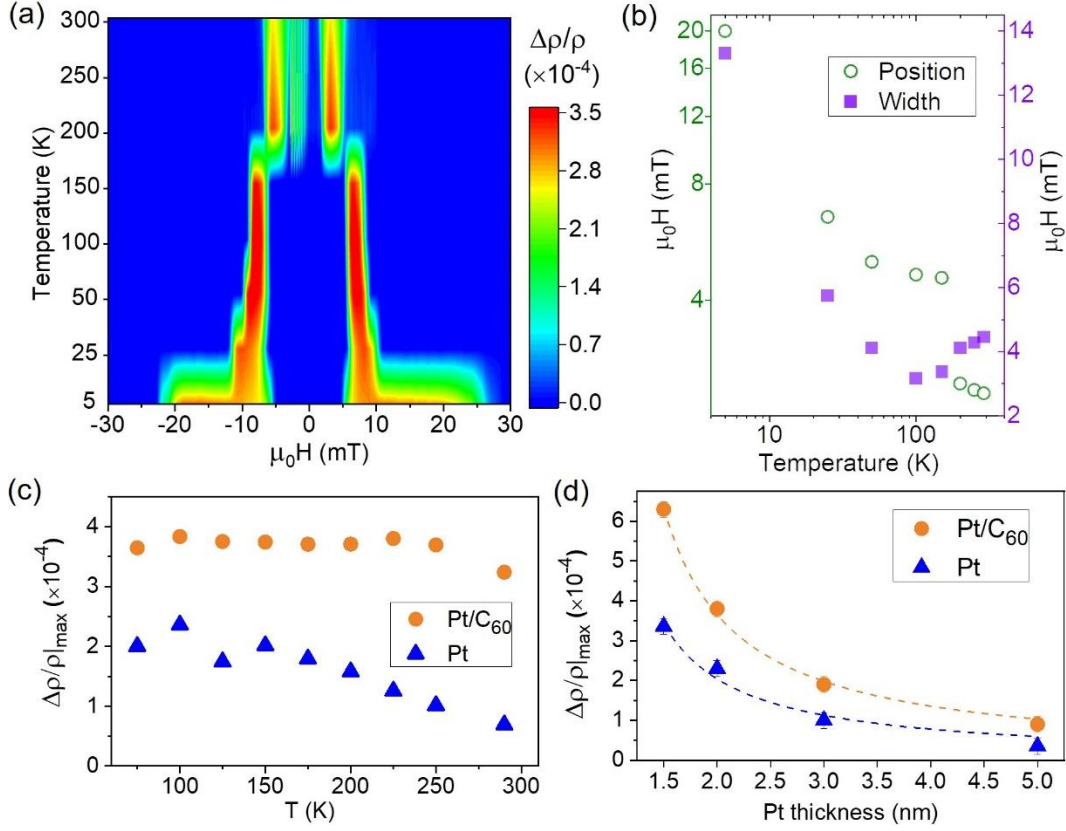


Figure 4. (a) Perpendicular LF-AMR for GGG/YIG(170)/Pt(2)/C₆₀(50). (b) As the sample is cooled, the perpendicular LF-AMR peak position and width are increased in steps, rather than monotonic fashion. (c) Temperature dependence of the maximum LF-AMR, calculated as the change in resistance from the peak in the perpendicular orientation to the minima in the longitudinal. There is a faster temperature drop in the MR values for Pt when compared with Pt/C₆₀. This may be due to the acquired magnetic moment in Pt/C₆₀ leading to a more stable induced magnetisation up to higher temperatures. (d) The LF-AMR for Pt and Pt/C₆₀ can be fitted to a $(t - x)^{-1}$ function, where t is the Pt wire thickness and x is a constant of 1 nm that we identify with the magnetically active Pt region.

CONCLUSIONS

Our results show that molecular overlayers can enhance the spin orbit coupling of heavy metals, as observed in both SHMR and AMR measurements. Additionally, the molecular layers aid in distinguishing the origin of spin scattering mechanisms, such as the coupling with YIG surface magnetisation and a LF-AMR measurable at high temperatures. The enhancement of the effective SOC with molecular interfaces has a wide range of applications, for example in reducing the current densities in spin transfer torque memories. Given the dependence on surface hybridisation and charge transfer, the SOC enhancement should be controllable with an applied electrical potential. This is an important development, as nearly all other methods to alter the spin-orbit coupling of a material are static. The inverse SHE can be modified by gating with ionic liquids, but changes to the SOC are undetermined and the electrical conversion may only be quenched⁴⁶. Materials can be doped during fabrication to increase the spin-orbit effect, but the effect is built-in and thus fixed with in a circuit. Using UHV grown nanoscale molecular films that can be gated offers a dynamic mechanism with the potential to alter the transport properties of an active circuit such as controlling the direction and magnitude of pure spin currents.

ASSOCIATED CONTENT

Additional information and figures on fabrication method, transport measurements, magnetometry and DFT simulations.

AUTHOR INFORMATION

Corresponding Author

*E-mail: o.cespedes@leeds.ac.uk

ACKNOWLEDGMENTS

This work was supported by Science Foundation Ireland [19/EP SRC/3605] and the Engineering and Physical Sciences Research Council (EPSRC) UK through grants EP/S030263, EP/K036408, EP/M000923, EP/I004483 and EP/S031081. This work made use of the ARCHER (via the UKCP Consortium, EPSRC UK EP/P022189/1 and EP/P022189/2), UK Materials and Molecular Modelling Hub (EPSRC UK EP/P020194/1) and STFC Scientific Computing Department's SCARF High-Performance Computing facilities. J.B. acknowledges support from the Royal Society through a University Research Fellowship. Electron microscopy work was carried out at SuperSTEM, the National Research Facility for Advanced Electron Microscopy supported by EPSRC. S.A. acknowledges support from Prince Sattam bin Abdulaziz University.

REFERENCES

- (1) Hellman, F.; Hoffmann, A.; Tserkovnyak, Y.; Beach, G. S. D.; Fullerton, E. E.; Leighton, C.; MacDonald, A. H.; Ralph, D. C.; Arena, D. A.; Durr, H. A.; Fischer, P.; Grollier, J.; Heremans, J. P.; Jungwirth, T.; Kimel, A. V.; Koopmans, B.; Krivorotov, I. N.; May, S. J.; Petford-Long, A. K.; Rondinelli, J. M.; Samarth, N.; Schuller, I. K.; Slavin, A. N.; Stiles, M. D.; Tchernyshyov, O.; Thiaville, A.; Zink, B. L. Interface-Induced Phenomena in Magnetism. *Rev. Mod. Phys.* **2017**, *89* (2), 025006.
- (2) Hueso, L. E.; Pruneda, J. M.; Ferrari, V.; Burnell, G.; Valdes-Herrera, J. P.; Simons, B. D.; Littlewood, P. B.; Artacho, E.; Fert, A.; Mathur, N. D. Transformation of Spin Information into Large Electrical Signals Using Carbon Nanotubes. *Nature* **2007**, *445* (7126), 410-413.
- (3) Liu, J.; Zhang, F. C.; Law, K. T. Majorana Fermion Induced Nonlocal Current Correlations in Spin-Orbit Coupled Superconducting Wires. *Phys. Rev. B* **2013**, *88* (6), 064509.
- (4) Shi, W. J.; Liu, J. W.; Xu, Y.; Xiong, S. J.; Wu, J.; Duan, W. H. Converting Normal Insulators into Topological Insulators via Tuning Orbital Levels. *Phys. Rev. B* **2015**, *92* (20), 205118.
- (5) Sinova, J.; Valenzuela, S. O.; Wunderlich, J.; Back, C. H.; Jungwirth, T. Spin Hall Effects. *Rev. Mod. Phys.* **2015**, *87* (4), 1213-1259.
- (6) Kang, M.-G.; Choi, J.-G.; Jeong, J.; Park, J. Y.; Park, H.-J.; Yuk, J. M.; Lee, K.-J.; Park, B.-G. Electric-Field Control of Field-Free Spin-Orbit Torque Switching via Laterally modulated Rashba Effect in Pt/Co/AlO_x Structures. *Resear Square (preprint)* **2020**, DOI: 10.21203/rs.3.rs-87924/v1.
- (7) Chen, Y. T.; Takahashi, S.; Nakayama, H.; Althammer, M.; Goennenwein, S. T. B.; Saitoh, E.; Bauer, G. E. W. Theory of Spin Hall Magnetoresistance. *Phys. Rev. B* **2013**, *87* (14), 144411.
- (8) Nakayama, H.; Althammer, M.; Chen, Y. T.; Uchida, K.; Kajiwara, Y.; Kikuchi, D.; Ohtani, T.; Geprags, S.; Opel, M.; Takahashi, S.; Gross, R.; Bauer, G. E. W.; Goennenwein, S. T. B.; Saitoh, E. Spin Hall Magnetoresistance Induced by a Nonequilibrium Proximity Effect. *Phys. Rev. Lett.* **2013**, *110* (20), 206601.
- (9) Althammer, M.; Meyer, S.; Nakayama, H.; Schreier, M.; Altmannshofer, S.; Weiler, M.; Huebl, H.; Geprags, S.; Opel, M.; Gross, R.; Meier, D.; Klewe, C.; Kuschel, T.; Schmalhorst, J. M.; Reiss, G.; Shen, L. M.; Gupta, A.; Chen, Y. T.; Bauer, G. E. W.; Saitoh, E.; Goennenwein, S. T. B. Quantitative Study of the Spin Hall Magnetoresistance in Ferromagnetic Insulator/Normal Metal Hybrids. *Phys. Rev. B* **2013**, *87* (22), 224401.

- (10) Hahn, C.; de Loubens, G.; Klein, O.; Viret, M.; Naletov, V. V.; Ben Youssef, J. Comparative Measurements of Inverse Spin Hall Effects and Magnetoresistance in YIG/Pt and YIG/Ta. *Phys. Rev. B* **2013**, *87* (17), 174417.
- (11) Althammer, M. Pure Spin Currents in Magnetically Ordered Insulator/Normal Metal Heterostructures. *J. Phys. D: Appl. Phys.* **2018**, *51* (30), 313001.
- (12) Fontcuberta, J.; Vasili, H. B.; Gazquez, J.; Casanova, F. On the Role of Interfaces on Spin Transport in Magnetic Insulator/Normal Metal Heterostructures. *Adv. Mater. Interfaces* **2019**, *6* (15), 1900475.
- (13) Wunderlich, J.; Kaestner, B.; Sinova, J.; Jungwirth, T. Experimental Observation of the Spin-Hall Effect in a Two-Dimensional Spin-Orbit Coupled Semiconductor System. *Phys. Rev. Lett.* **2005**, *94* (4), 047204.
- (14) Isasa, M.; Villamor, E.; Hueso, L. E.; Gradhand, M.; Casanova, F. Temperature Dependence of Spin Diffusion Length and Spin Hall Angle in Au and Pt. *Phys. Rev. B* **2015**, *91* (2), 024402.
- (15) Qu, D.; Huang, S. Y.; Miao, B. F.; Huang, S. X.; Chien, C. L. Self-Consistent Determination of Spin Hall Angles in Selected 5d Metals by Thermal Spin Injection. *Phys. Rev. B* **2014**, *89* (14), 140407.
- (16) Liu, L. Q.; Moriyama, T.; Ralph, D. C.; Buhrman, R. A. Spin-Torque Ferromagnetic Resonance Induced by the Spin Hall Effect. *Phys. Rev. Lett.* **2011**, *106* (3), 036601.
- (17) Lu, Y. M.; Choi, Y.; Ortega, C. M.; Cheng, X. M.; Cai, J. W.; Huang, S. Y.; Sun, L.; Chien, C. L. Pt Magnetic Polarization on Y3Fe5O12 and Magnetotransport Characteristics. *Phys. Rev. Lett.* **2013**, *110* (14), 147207.
- (18) Geprags, S.; Meyer, S.; Altmannshofer, S.; Opel, M.; Wilhelm, F.; Rogalev, A.; Gross, R.; Goennenwein, S. T. B. Investigation of induced Pt magnetic polarization in Pt/Y3Fe5O12 bilayers. *Appl. Phys. Lett.* **2012**, *101* (26), 262407.
- (19) Atodiresei, N.; Raman, K. V. Interface-Assisted Spintronics: Tailoring at the Molecular Scale. *MRS Bull.* **2014**, *39* (7), 596-601.
- (20) Cespedes, O.; Ferreira, M. S.; Sanvito, S.; Kociak, M.; Coey, J. M. D. Contact Induced Magnetism in Carbon Nanotubes. *Journal of Physics-Condensed Matter* **2004**, *16* (10), L155-L161.
- (21) Cinchetti, M.; Dediu, V. A.; Hueso, L. E. Activating the Molecular Spinterface. *Nat. Mater.* **2017**, *16*, 507-515.
- (22) Bairagi, K.; Bellec, A.; Repain, V.; Chacon, C.; Girard, Y.; Garreau, Y.; Lagoute, J.; Rousset, S.; Breitwieser, R.; Hu, Y. C.; Chao, Y. C.; Pai, W. W.; Li, D.; Smogunov, A.; Barreteau, C. Tuning the Magnetic Anisotropy at a Molecule-Metal Interface. *Phys. Rev. Lett.* **2015**, *114* (24), 247203.
- (23) Ma'Mari, F. A.; Moorsom, T.; Teobaldi, G.; Deacon, W.; Prokscha, T.; Leutkens, H.; Lee, S.; Sterbinsky, G. E.; Arena, D. A.; MacLaren, D. A.; Flokstra, M.; Ali, M.; Wheeler, M. C.; Burnell, G.; Hickey, B. J.; Cespedes, O. Beating the Stoner Criterion Using Molecular Interfaces. *Nature* **2015**, *524*, 69-73.
- (24) Al Ma'Mari, F.; Rogers, M.; Alghamdi, S.; Moorsom, T.; Lee, S.; Prokscha, T.; Luetkens, H.; Valvidares, M.; Teobaldi, G.; Flokstra, M.; Stewart, R.; Gargiani, P.; Ali, M.; Burnell, G.; Hickey, B. J.; Cespedes, O. Emergent Magnetism at Transition-Metal-Nanocarbon Interfaces. *Proc. Natl. Acad. Sci. U.S.A.* **2017**, *114* (22), 5583-5588.
- (25) Djeghloul, F.; Gruber, M.; Urbain, E.; Xenioti, D.; Joly, L.; Boukari, S.; Arabski, J.; Bulou, H.; Scheurer, F.; Bertran, F.; Fevre, P. L.; Taleb-Ibrahimi, A.; Wulfhekel, W.; Garreau, G.; Hajjar-Garreau, S.; Wetzels, P.; Alouani, M.; Beaurepaire, E.; Bowen, M.; Weber, W. High Spin Polarization at Ferromagnetic Metal-Organic Interfaces: A Generic Property. *The Journal of Physical Chemistry Letters* **2016**, *7*, 2310 - 2315.
- (26) Raman, K. V.; Kamerbeek, A. M.; Mukherjee, A.; Atodiresei, N.; Sen, T. K.; Lazic, P.; Caciuc, V.; Michel, R.; Stalke, D.; Mandal, S. K.; Bluegel, S.; Muenzenberg, M.; Moodera, J. S. Interface-Engineered Templates for Molecular Spin Memory Devices. *Nature* **2013**, *493* (7433), 509-513.
- (27) Moorsom, T.; Wheeler, M.; Kahn, T. M.; Ma'Mari, F. A.; Kinane, C.; Langridge, S.; Ciudad, D.; Bedoya-Pinto, A.; Hueso, L.; Teobaldi, G.; Lazarov, V. K.; Gilks, D.; Burnell, G.; Hickey, B. J.; Cespedes, O. Spin-Polarized Electron Transfer in Ferromagnet/C₆₀ Interfaces. *Phys. Rev. B* **2014**, *90* (12), 125311.

- (28) Moorsom, T.; Alghamdi, S.; Stansill, S.; Poli, E.; Teobaldi, G.; Beg, M.; Fangohr, H.; Rogers, M.; Aslam, Z.; Ali, M.; Hickey, B. J.; Cespedes, O. π -Anisotropy: A Nanocarbon Route to Hard Magnetism. *Phys. Rev. B* **2020**, *101* (6), 060408.
- (29) Sun, D.; van Schooten, K. J.; Kavand, M.; Malissa, H.; Zhang, C.; Groesbeck, M.; Boehme, C.; Vardeny, Z. V. Inverse Spin Hall Effect From Pulsed Spin Current in Organic Semiconductors with Tunable Spin-Orbit Coupling. *Nat. Mater.* **2016**, *15* (8), 863-869.
- (30) Das, R.; Kalappattil, V.; Geng, R.; Luong, H.; Pham, M.; Nguyen, T.; Liu, T.; Wu, M. Z.; Phan, M. H.; Srikanth, H. Enhanced Room-Temperature Spin Seebeck Effect in a YIG/C₆₀/Pt Layered Heterostructure. *AIP Adv.* **2018**, *8* (5), 055906.
- (31) Wheeler, M. C.; Al Ma'Mari, F.; Rogers, M.; Goncalves, F. J.; Moorsom, T.; Brataas, A.; Stamps, R.; Ali, M.; Burnell, G.; Hickey, B. J.; Cespedes, O. Optical Conversion of Pure Spin Currents in Hybrid Molecular Devices. *Nat. Commun.* **2017**, *8*, 926.
- (32) Grosser, M.; Schmid, U. The Impact of Sputter Conditions on the Microstructure and on the Resistivity of Tantalum Thin Films. *Thin Solid Films* **2009**, *517* (16), 4493-4496.
- (33) Velez, S.; Golovach, V. N.; Bedoya-Pinto, A.; Isasa, M.; Sagasta, E.; Abadia, M.; Rogero, C.; Hueso, L. E.; Bergeret, F. S.; Casanova, F. Hanle Magnetoresistance in Thin Metal Films with Strong Spin-Orbit Coupling. *Phys. Rev. Lett.* **2016**, *116* (1), 016603.
- (34) Marmion, S. R.; Ali, M.; McLaren, M.; Williams, D. A.; Hickey, B. J. Temperature Dependence of spin Hall Magnetoresistance in Thin YIG/Pt Films. *Phys. Rev. B* **2014**, *89* (22), 220404.
- (35) Meyer, S.; Althammer, M.; Geprags, S.; Opel, M.; Gross, R.; Goennenwein, S. T. B. Temperature Dependent Spin Transport Properties of Platinum Inferred from Spin Hall Magnetoresistance Measurements. *Appl. Phys. Lett.* **2014**, *104* (24), 242411.
- (36) Zhang, X. P.; Bergeret, F. S.; Golovach, V. N. Theory of Spin Hall Magnetoresistance from a Microscopic Perspective. *Nano Lett.* **2019**, *19* (9), 6330-6337.
- (37) Tserkovnyak, Y.; Brataas, A.; Bauer, G. E. W. Spin Pumping and Magnetization Dynamics in Metallic Multilayers. *Phys. Rev. B* **2002**, *66* (22), 224403.
- (38) Choi, J. G.; Lee, J. W.; Park, B. G. Spin Hall Magnetoresistance in Heavy-Metal/Metallic-Ferromagnet Multilayer Structures. *Phys. Rev. B* **2017**, *96* (17), 174412.
- (39) Friedrich, R.; Caciuc, V.; Bihlmayer, G.; Atodiresei, N.; Blugel, S. Designing the Rashba Spin Texture by Adsorption of Inorganic Molecules. *New J. Phys.* **2017**, *19*, 043017.
- (40) Isasa, M.; Martinez-Velarte, M. C.; Villamor, E.; Magen, C.; Morellon, L.; De Teresa, J. M.; Ibarra, M. R.; Vignale, G.; Chulkov, E. V.; Krasovskii, E. E.; Hueso, L. E.; Casanova, F. Origin of Inverse Rashba-Edelstein Effect Detected at the Cu/Bi Interface Using Lateral Spin Valves. *Phys. Rev. B* **2016**, *93* (1), 014420.
- (41) Jakobs, S.; Narayan, A.; Stadtmuller, B.; Droghetti, A.; Rungger, I.; Hor, Y. S.; Klyatskaya, S.; Jungkenn, D.; Stockl, J.; Laux, M.; Monti, O. L. A.; Aeschlimann, M.; Cava, R. J.; Ruben, M.; Mathias, S.; Sanvito, S.; Cinchetti, M. Controlling the Spin Texture of Topological Insulators by Rational Design of Organic Molecules. *Nano Lett.* **2015**, *15* (9), 6022-6029.
- (42) Rojas Sanchez, J. C.; Vila, L.; Desfonds, G.; Gambarelli, S.; Attane, J. P.; De Teresa, J. M.; Magen, C.; Fert, A. Spin-to-Charge Conversion Using Rashba Coupling at the Interface Between Non-Magnetic Materials. *Nat. Commun.* **2013**, *4*, 2944.
- (43) Mitra, A.; Cespedes, O.; Ramasse, Q.; Ali, M.; Marmion, S.; Ward, M.; Brydson, R. M. D.; Kinane, C. J.; Cooper, J. F. K.; Langridge, S.; Hickey, B. J. Interfacial Origin of the Magnetisation Suppression of Thin Film Yttrium Iron Garnet. *Sci. Rep.* **2017**, *7*, 11774.
- (44) Corte-Leon, H.; Nabaei, V.; Manzin, A.; Fletcher, J.; Krzysteczko, P.; Schumacher, H. W.; Kazakova, O. Anisotropic Magnetoresistance State Space of Permalloy Nanowires with Domain Wall Pinning Geometry. *Sci. Rep.* **2014**, *4*, 6045.
- (45) Gil, W.; Gortlitz, D.; Horisberger, M.; Kotzler, J. Magnetoresistance Anisotropy of Polycrystalline Cobalt Films: Geometrical-Size and Domain Effects. *Phys. Rev. B* **2005**, *72* (13), 134401.

(46) Dushenko, S.; Hokazono, M.; Nakamura, K.; Ando, Y.; Shinjo, T.; Shiraishi, M. Tunable Inverse Spin Hall Effect in Nanometer-Thick Platinum Films by Ionic Gating. *Nat. Commun.* **2018**, *9*, 3118.

For Table of Contents Only

